*Supplement of*

# Estimation of Canada's methane emissions: inverse modelling analysis using the ECCC measurement network

Misa Ishizawa, Douglas Chan, Doug Worthy, Elton Chan, Felix Vogel, Joe R. Melton, and Vivek K. Arora

Climate Research Division, Environment and Climate Change Canada, Canada

*Correspondence to:* Misa Ishizawa (misa.ishizawa@ec.gc.ca) and Douglas Chan (douglas.chan@ec.gc.ca)

## S1. Site Descriptions

**Alert (ALT, 82.5° N, 62.5° W), Nunavut,** has been referred to as an Arctic background site, being located thousands of kilometres from major source regions. The Alert observatory is ~6 km away from the military base camp. The lack of local source surrounding the site results in no significant diurnal variation in observed atmospheric $CH_4$ concentrations all year around. In the winter, under weak vertical mixing, well-defined synoptic variations are observed due to inter-continental scale transport along with mainly anthropogenic $CH_4$ originating from the Eurasia continent (Worthy et al., 2009). The measurements at Alert can represent the large-scale background conditions like long-term trend and mean seasonal cycle in the Arctic (Worthy et al., 2009).

**Behchoko (BCK, 62.8° N, 115.9° W), Northwest Territories,** is located on the northwest tip of Great Slave Lake. The continuous measurement was started in October 2012. The air sampling intake is at the top of a 60 m communication tower in a local power generation station: 10 km away from the town of Behchoko, a community ~80 km northwest of Yellowknife, the capital of Northwest Territories. Mixed forests, lakes and ponds surround BCK.

**Chibougamau (CHM, 49.7° N, 74.3° W) and Chapais (CPS, 49.8N, 75.0W), Quebec:** CHM is surrounded by boreal forest and lakes, located 30 km south of the town of Chibougamau in central Quebec. CHM's continuous GHG measurement program started in August 2007 and was replaced with CPS in 2011. CPS is located ~45 km northwest of CHM, 10 km north of the town of Chapais. The air sampling was started at an 8 m tower and then moved to a 40 m tower in September 2014.

**Churchill (CHL, 58.7° N, 93.8 ° W), Manitoba,** is located on the west coast of Hudson Bay. The GHG monitoring program began with flask air sampling in 2007 before the continuous measurement system started in October 2011. The sampling equipment is installed in the Churchill Northern Studies Research Facility, ~23 km east of Churchill. CHL is situated with Arctic tundra to the north and in the northern perimeter of the Hudson Bay Lowland, the largest boreal wetland in North America.

**Downsview (DWS, 43.8° N, 79.5° W), Ontario,** is located in the ECCC GHG laboratory. DWS is in the suburbs of Toronto, ~15 km north of the downtown, surrounded by a mixture of residential and industrial areas with the adjacent green space in the south. The air sampling intake is installed 20 m above ground, on the top of the laboratory building. Continuous measurement has been steadily operated since 2012.

**East Trout Lake (ETL, 54.4° N, 105° W), Saskatchewan,** is located near the southern edge of the boreal forest**,** ~140 km north of the closest town, Prince Albert. ETL started in 2005 as a replacement for Candle Lake (CDL), south of 50 km of ETL. CDL began in 2002 as a part of the Boreal Ecosystem Research and Monitoring Site (BERMS) and Fluxnet Canada research program. The air sampling intake is installed on a 105 m communication tower.

**Egbert (EGB, 44.2° N, 79.8° W), Ontario,** is ~100 km north of Toronto, on the campus of the Centre for Atmospheric Research Experiments (CARE), a laboratory of ECCC. As a regionally representative site, EGB provides the infrastructure for long-term atmospheric observations of air quality, tropospheric ozone, and greenhouse gases. The GHG measurement started in March 2005.

**Estevan Point (ESP, 49.6° N, 126.4° W**), **British Colombia**, is located on the west coast of Vancouver Island. The site faces the Pacific Ocean on the west and is surrounded by forests. A weekly sampling of $CO_2$ started in 1992 and $CH_4$ in 1998. In April 2009, a continuous measurement system was installed.

**Fraserdale (FSD, 49.9° N, 81.6° W), Ontario,** is located on the southern perimeter of the Hudson Bay Lowland and on the northern edge of the boreal forest. The site was established in December 1989 as part of the Northern Wetlands Study (NOWES) to assess the role of northern wetlands in the exchange of atmospheric trace gases (Glooschenko et al., 1994). The air is sampled on a 40 m tower at the east end of a 1 $km^2$ clearing and a reservoir of a hydroelectric generating dam. A more detailed site description can be found elsewhere (Worthy et al., 1998).

**Inuvik (INU, 68.3° N, 133.5° W), Northwest Territories,** is ~120 km south of the coast of the Arctic Ocean. The continuous measurement was started in February 2012, followed by flask sampling in May 2012. The measurement system is located in the ECCC upper air weather station building, 5 km southeast of the town of Inuvik. INU is ecologically surrounded by Arctic tundra and geologically located in the east channel of the Mackenzie Delta, where a number of water streams and ponds are formed and vast hydrocarbon deposits are found. Although there are proposed developments of natural gas and pipeline projects, they have been on hold.

**Lac La Biche (LLB, 54.9° N, 112.5° W), Alberta,** is located in a region of peatland and forest, 200 km northeast of Edmonton, the capital of the province of Alberta. The Athabasca oil sands are 230 km north of LLB. High $CH_4$ concentrations are often observed, especially in the winter season when wetland $CH_4$ signals are weak. The winter high $CH_4$ signals are considered to be associated with oil industry south of LLB (Lopez et al., 2017). The greenhouse gas monitoring program started in April 2007, with continuous measurements of $CO_2$, $CH_4$ and CO.

**Sable Island (WSA, 43.9° N, 60.0° W), Nova Scotia**, is on a small island, 40 km long and 1 km wide, in the Northern Atlantic Ocean. ~275 km east-southeast of Halifax, Nova Scotia. $CO_2$ measurements were started in 1992, and $CH_4$ measurements in 1999. In contrast to ESP on the Pacific coast, WSA is east of the North American continent, facing the Atlantic. WSA is thus located downstream of the North American continent, continuously influenced by the complex meteorology of synoptic systems with air masses from the regions in Canada and US, where high anthropogenic sources and biospheric flux sources are located (Worthy et al., 2003). For some sampling issues, the measurements were on pause for nearly three years, from early 2014 to early 2017. In March 2017, the continuous measurement was resumed.

## References

Glooschenko, W. A., Roulet, N. T., Barrie, L. A., Schiff, H. I., and McAdie, H. G.: The Northern Wetlands Study (NOWES): An overview, J. Geophys. Res., 99, 1423-1428, https://doi.org/10.1029/93JD02184, 1994.

Lopez, M., Sherwood, O. A., Dlugokencky, E. J., Kessler, R., Giroux, L., and Worthy, D. E. J.: Isotopic signatures of anthropogenic CH4 sources in Alberta, Canada, Atmos. Environ., 164, 280-288, https://doi.org/10.1016/j.atmosenv.2017.06.021, 2017.

Worthy, D. E. J., Higuchi, K., and Chan, D.: North American influence on atmospheric carbon dioxide data collected at Sable Island, Canada, Tellus B: Chemical and Physical Meteorology, 55, 105-114, 10.3402/tellusb.v55i2.16731, 2003.

Worthy, D. E. J., Levin, I., Trivett, N. B. A., Kuhlmann, A. J., Hopper, J. F., and Ernst, M. K.: Seven years of continuous methane observations at a remote boreal site in Ontario, Canada, J. Geophys. Res., 103, 15995-16007, 10.1029/98jd00925, 1998.

Worthy, D. E. J., Chan, E., Ishizawa, M., Chan, D., Poss, C., Dlugokencky, E. J., Maksyutov, S., and Levin, I.: Decreasing anthropogenic methane emissions in Europe and Siberia inferred from continuous carbon dioxide and methane observations at Alert, Canada, J. Geophys. Res., 114, 10.1029/2008JD011239, 2009.

**Table S1.** Experiments per inversion setup in this study

| Experiments | | | |
|---|---|---|---|
| Prior fluxes[1] | Transport Models | | |
| | **FLEXPART_EI** | **FLEXPART_JRA55** | **WRF-STILT** |
| **WetCHARTs_ECAQ** | WetCHARTs_ECAQ_FLEX_EI | WetCHARTs_ECAQ_FLEX_JRA | WetCHARTs_ECAQ_STILT |
| **WetCHARTs_EDGAR** | WetCHARTs_EDGAR_FLEX_EI | WetCHARTs_EDGAR_FLEX_JRA | WetCHARTs_EDGAR_STILT |
| **GCPwet_ECAQ** | GCPwet_ECAQ_FLEX_EI | GCPwet_ECAQ_FLEX_JRA | GCPwet_ECAQ_STILT |
| **GCPwet_EDGAR** | GCPwet_EDGAR_FLEX_EI | GCPwet_EDGAR_FLEX_JRA | GCPwet_EDGAR_STILT |
| **CLASSICdiag_ECAQ** | CLASSICdiag_ECAQ_FLEX_EI | CLASSICdiag_ECAQ_FLEX_JRA | CLASSICdiag_ECAQ_STILT |
| **CLASSICdiag_EDGAR** | CLASSICdiag_EDGAR_FLEX_EI | CLASSICdiag_EDGAR_FLEX_JRA | CLASSICdiag_EDGAR_STILT |
| **CLASSICprog_ECAQ** | CLASSICprog_ECAQ_FLEX_EI | CLASSICprog_ECAQ_FLEX_JRA | CLASSICprog_ECAQ_STILT |
| **CLASSICprog_EDGAR** | CLASSICprog_EDGAR_FLEX_EI | CLASSICprog_EDGAR_FLEX_JRA | CLASSICprog_EDGAR_STILT |

[1]Eight scenarios of prior emission consist of four different wetland fluxes and two anthropogenic emission inventories, which are listed in Table 2.

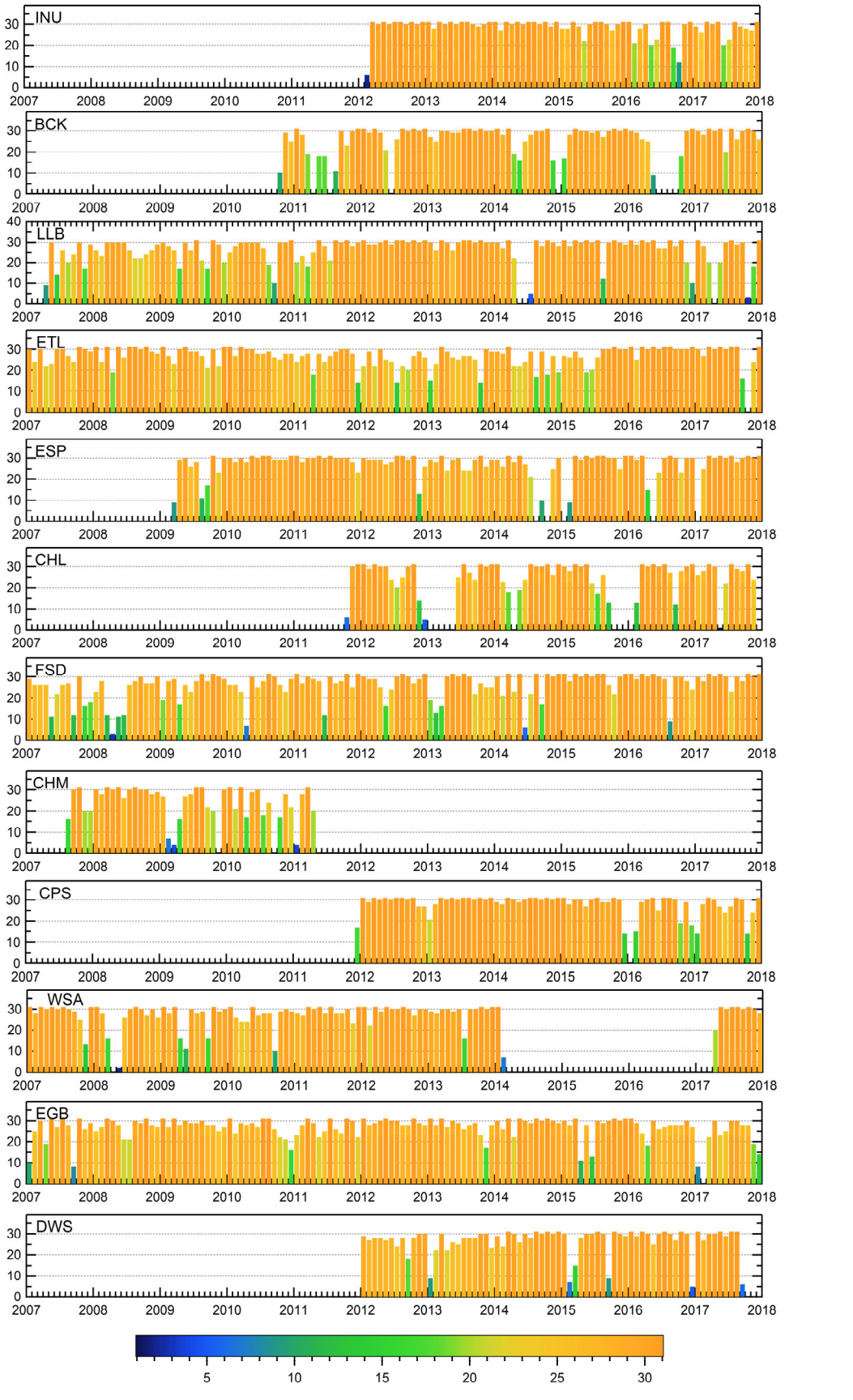


**Figure S1**. Data availability at the 12 sites used for inversion in this study.

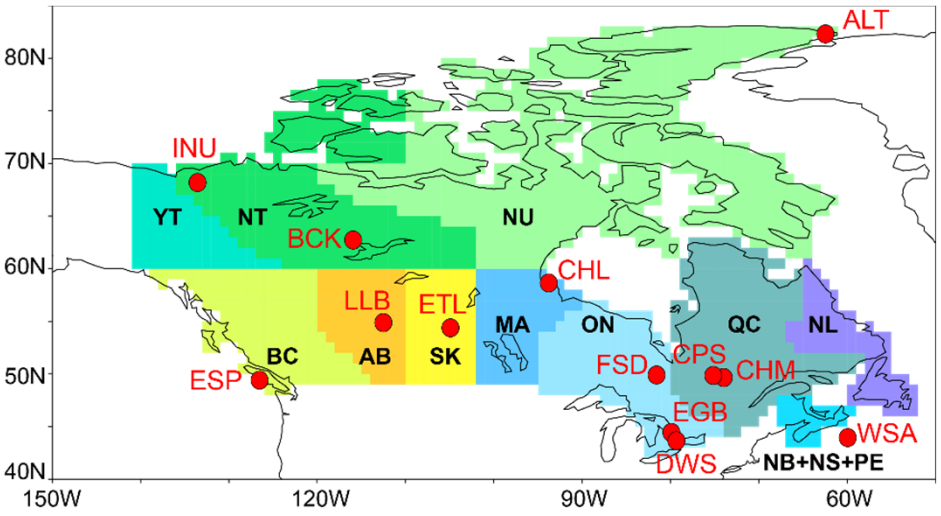


**Figure S2.** ECCC Measurement sites (site ID in red) used in this study and Canadian provinces and territories. There are 13 provinces/territories: Yukon (YT), Northwest Territories (NT), Nunavut (NU), British Columbia (BC), Alberta (AB), Saskatchewan (SK), Manitoba (MB), Ontario(ON), Quebec (QC), New Brunswick (NB), Nova Scotia (NS), Prince Edward Island (PE), Newfoundland and Labrador (NL).

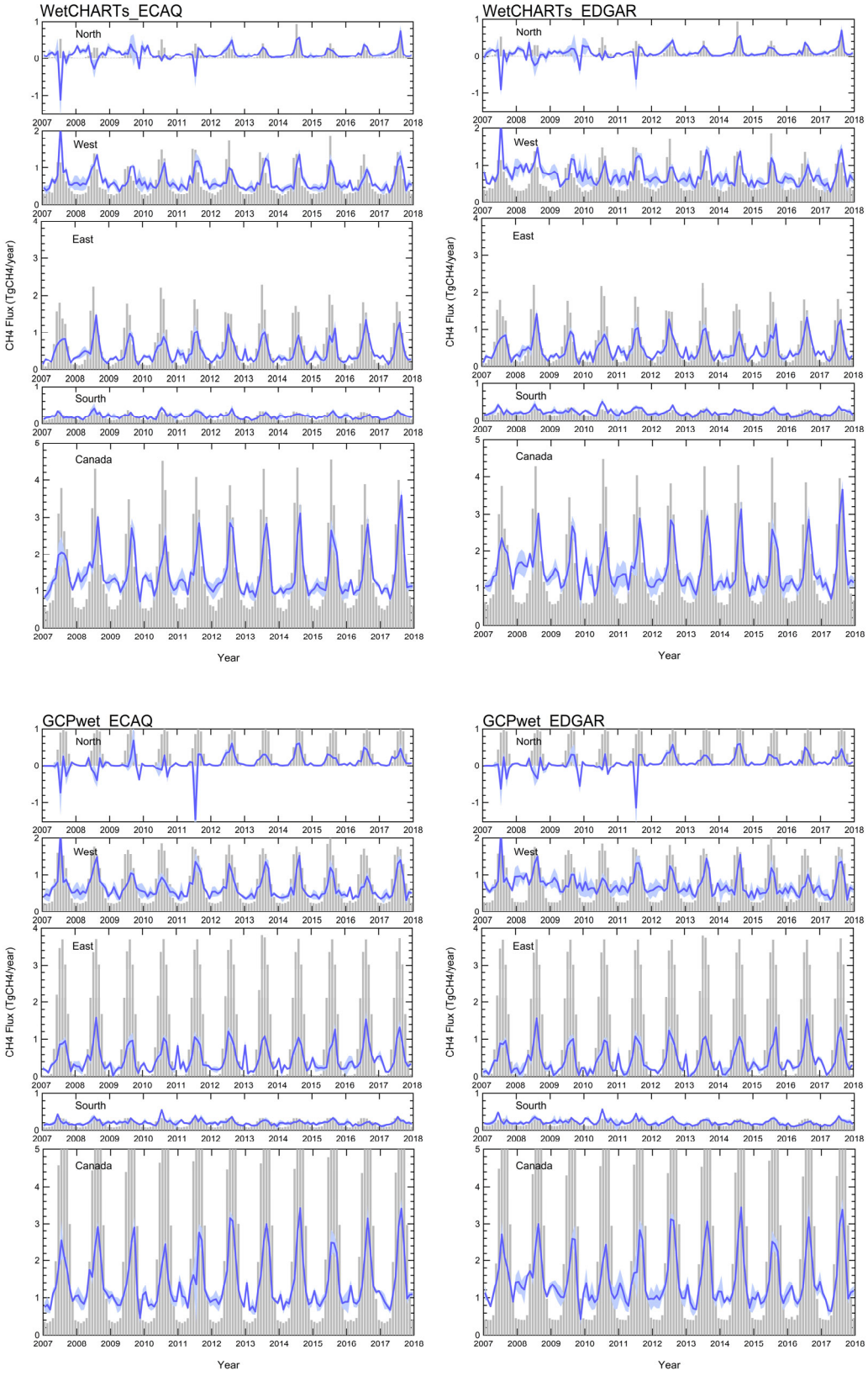


**Figure S3**. Monthly posterior $CH_4$ fluxes for subregions and Canada in reference inversion, Inv_4R12S. The blue lines are the mean posterior fluxes of experiments with three transport models (FLEXPART_EI, FLEXPART_JRA, and WRF-STILT) with prior emission scenarios of WetCHARTs_ECAQ, WetCHARTs_EDGAR, GCPwet_ECAQ and GCPwet_EDGAR. The shaded areas indicate the min-max ranges of the posterior fluxes over respective experiments (see Table S1).

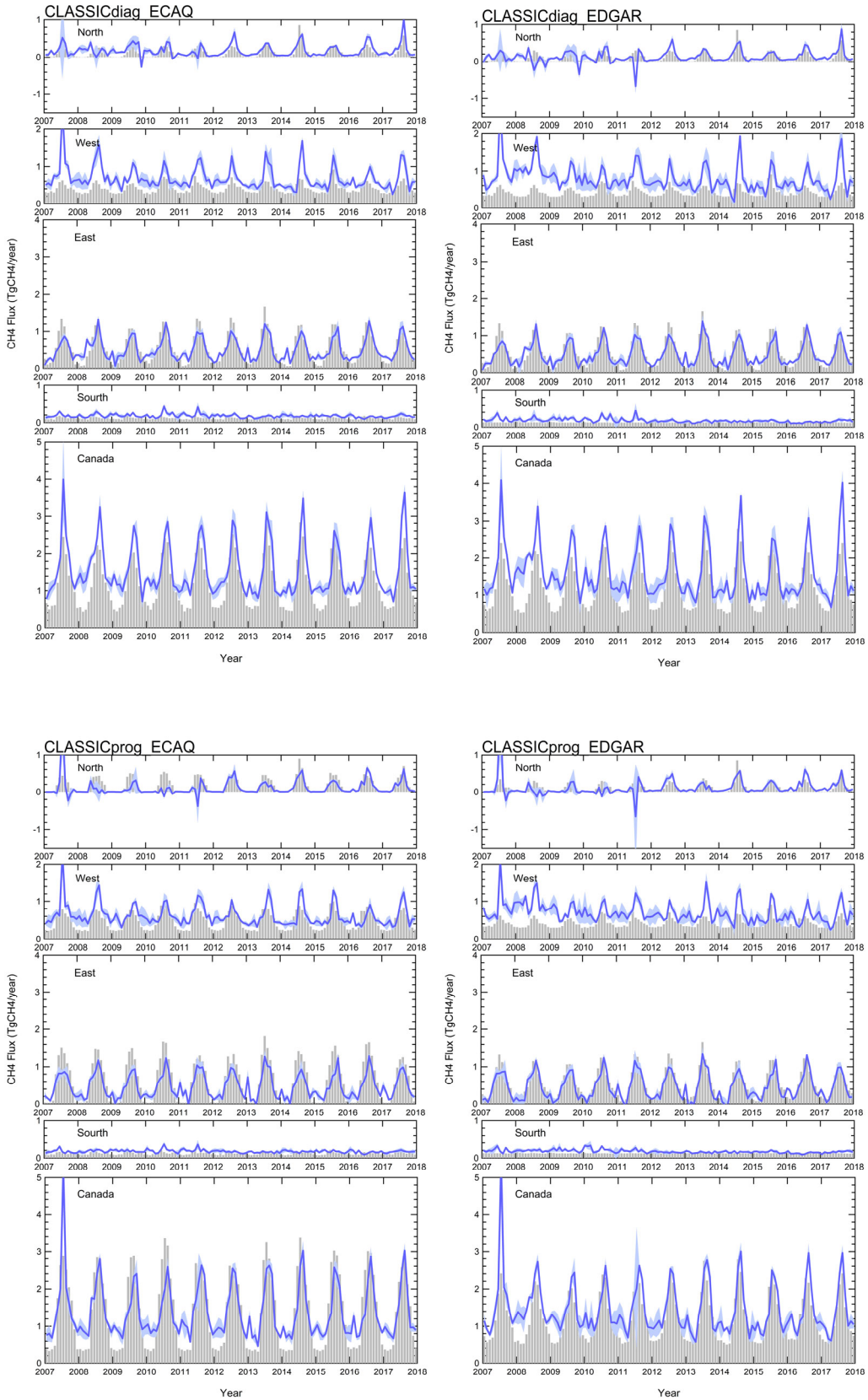


**Figure S3 (continued).** Same but with prior emission scenarios of CLASSICdiag_ECAQ, CLASSICdiag_EDGAR, CLASSICprog_ECAQ and CLASSICprog_EDGAR.

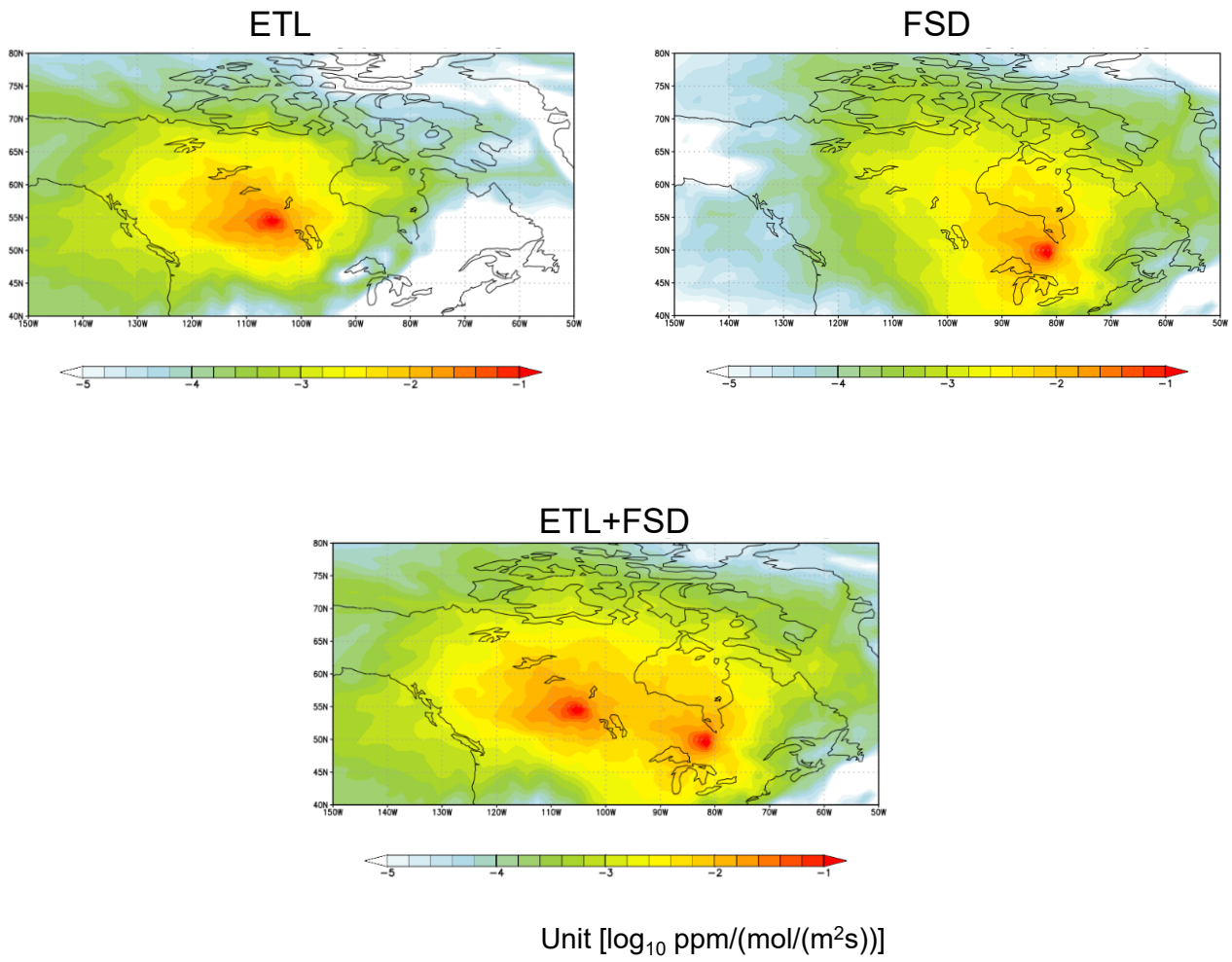


**Figure S4.** Examples of annual mean footprints of ETL (East Trout Lake) and FSD (Faserdale), individually and combined, by FLEXPART-EI for 2015.

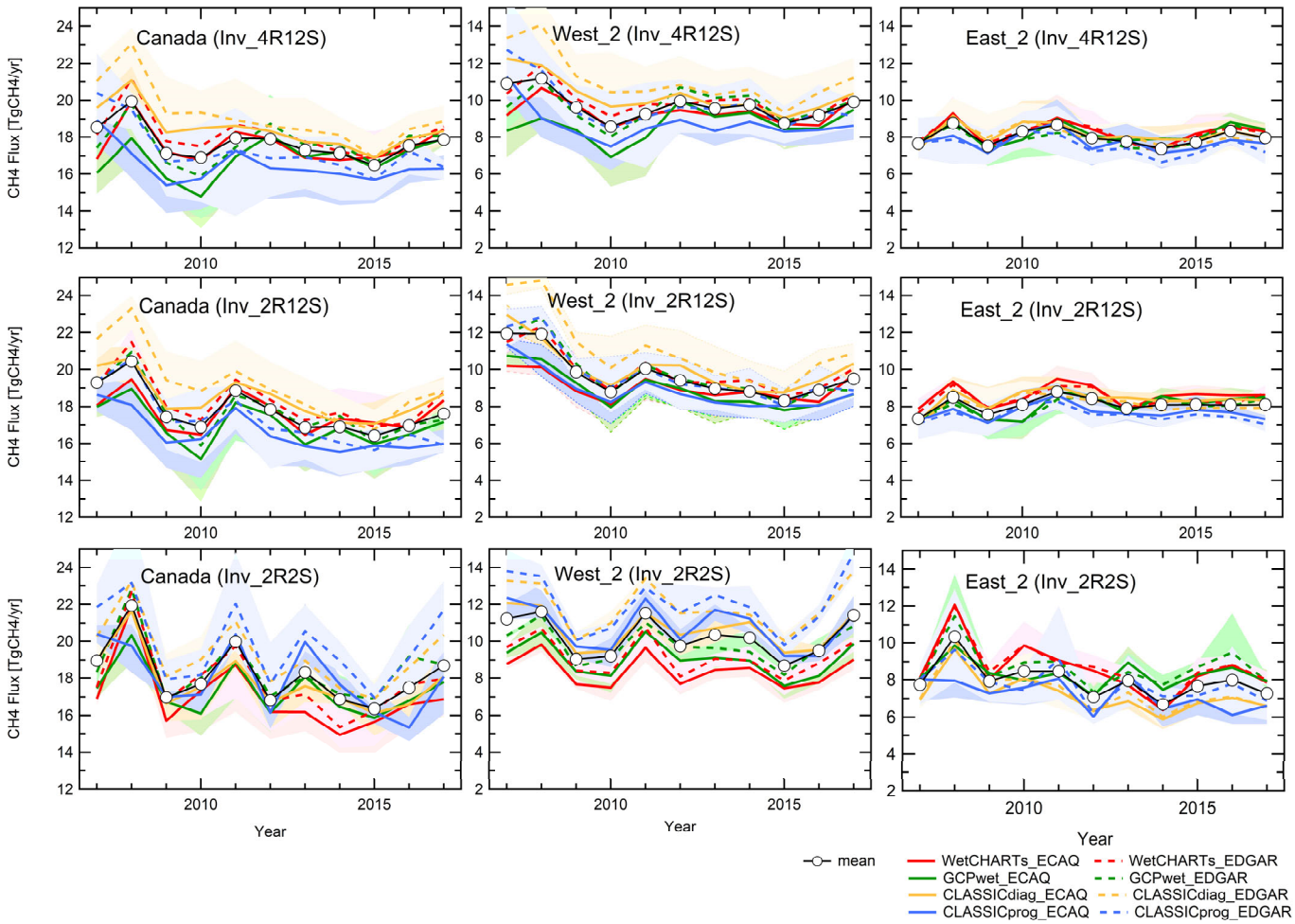


**Figure S5.** Trends of estimated yearly CH4 fluxes for Canada and western and eastern regions (West_2 and East_2) per inversion setup of regional mask and site selections (Inv_4R12S uses four subregions and 12 sites, Inv_2R12S uses two subregions and 12 sites, Inv_2R2S uses two subregions and 2 sites). The subregion masks and observation sites are defined in Fig. 4. Black solid lines with open circles indicate the mean fluxes of each inversion setup. Solid and dotted lines show each mean flux over three different transports per prior flux scenario. The shaded areas indicate the min-max ranges of the posterior fluxes over three experiments per prior flux scenario. The inversion experiments with prior scenarios and transport models are defined in Table S1.

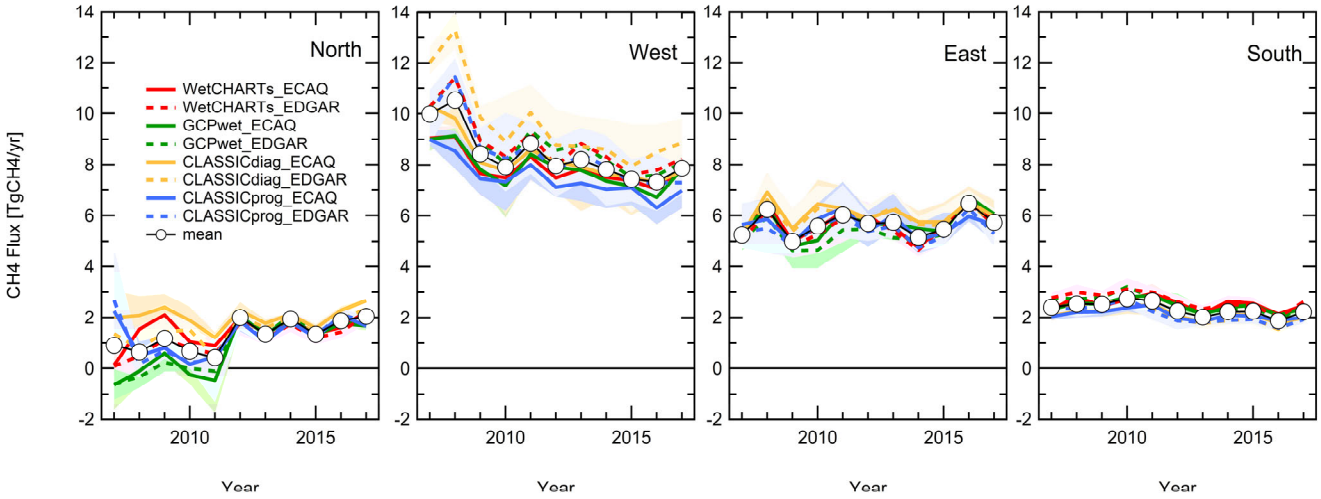


**Figure S6.** Trends of estimated yearly $CH_4$ fluxes for four subregions (North, West, East and South) through the reference inversion, Inv_4R12S. Black solid lines with open circles indicate the mean trend over 24 experiments. The other solid and dotted lines show mean fluxes over three different transports per prior emission scenario. The shaded areas indicate the min-max ranges of the posterior fluxes over three experiments per prior flux scenario.

**Table S2.** Ensemble mean trends of estimated yearly $CH_4$ fluxes and uncertainties (SD among the ensembles) for Canada and western (West_2) and eastern (East_2) regions from three inversion setups, 72 experiments in total and 24 experiments in each of three inversion setups (Inv_4R12S, Inv_2R12S and Inv_2R2S) with different subregion masks and observation site selections. The trends are calculated as slopes of linear fit over three periods: the whole (2007–2017), the early (2007–2011) and the later (2012–2017) periods.

| | **Canada** | | | **West_2** | | | **East_2** | | |
|---|---|---|---|---|---|---|---|---|---|
| | 2007–2017 | 2007–2011 | 2012–2017 | 2007–2017 | 2007–2011 | 2012–2017 | 2007–2017 | 2007–2011 | 2012–2017 |
| **Total** | -0.20 (0.14) | -0.36 (0.59) | 0.05 (0.23) | -0.15 (0.14) | -0.49 (0.48) | 0.02 (0.17) | -0.05 (0.10) | 0.02 (0.27) | 0.03 (0.12) |
| **Inv_4R12S** | -0.14 (0.18) | -0.42 (0.68) | 0.00 (0.19) | -0.12 (0.14) | -0.59 (0.53) | -0.07 (0.14) | -0.02 (0.06) | 0.16 (0.22) | -0.02 (0.04) |
| **Inv_2R12S** | -0.25 (0.13) | -0.44 (0.62) | -0.04 (0.22) | -0.27 (0.13) | -0.70 (0.47) | -0.01 (0.15) | 0.03 (0.06) | 0.25 (0.22) | -0.03 (0.10) |
| **Inv_2R2S** | -0.22 (0.08) | -0.22 (0.43) | 0.18 (0.23) | -0.07 (0.05) | -0.18 (0.26) | 0.12 (0.16) | -0.15 (0.08) | -0.04 (0.29) | 0.06 (0.11) |

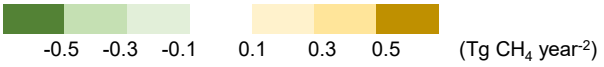

**Table S3.** Correlation coefficients and *p*-values of estimated ensemble mean yearly $CH_4$ fluxes between subregions and between subregion and Canada. The analysis period is from 2012 to 2012.

| | North | West | East | South | Canada |
|---|---|---|---|---|---|
| North | | $r = 0.37$<br>$p = 0.46$ | $r = 0.41$<br>$p = 0.42$ | $r = -0.12$<br>$p = 0.82$ | $r = 0.74$<br>$p = 0.09$ |
| West | | | $r = -0.38$<br>$p = 0.45$ | $r = 0.25$<br>$p = 0.63$ | $r = 0.37$<br>$p = 0.46$ |
| East | | | | $r = -0.82$<br>$p = 0.05$ | $r = 0.41$<br>$p = 0.42$ |
| South | | | | | $r = -0.12$<br>$p = 0.82$ |

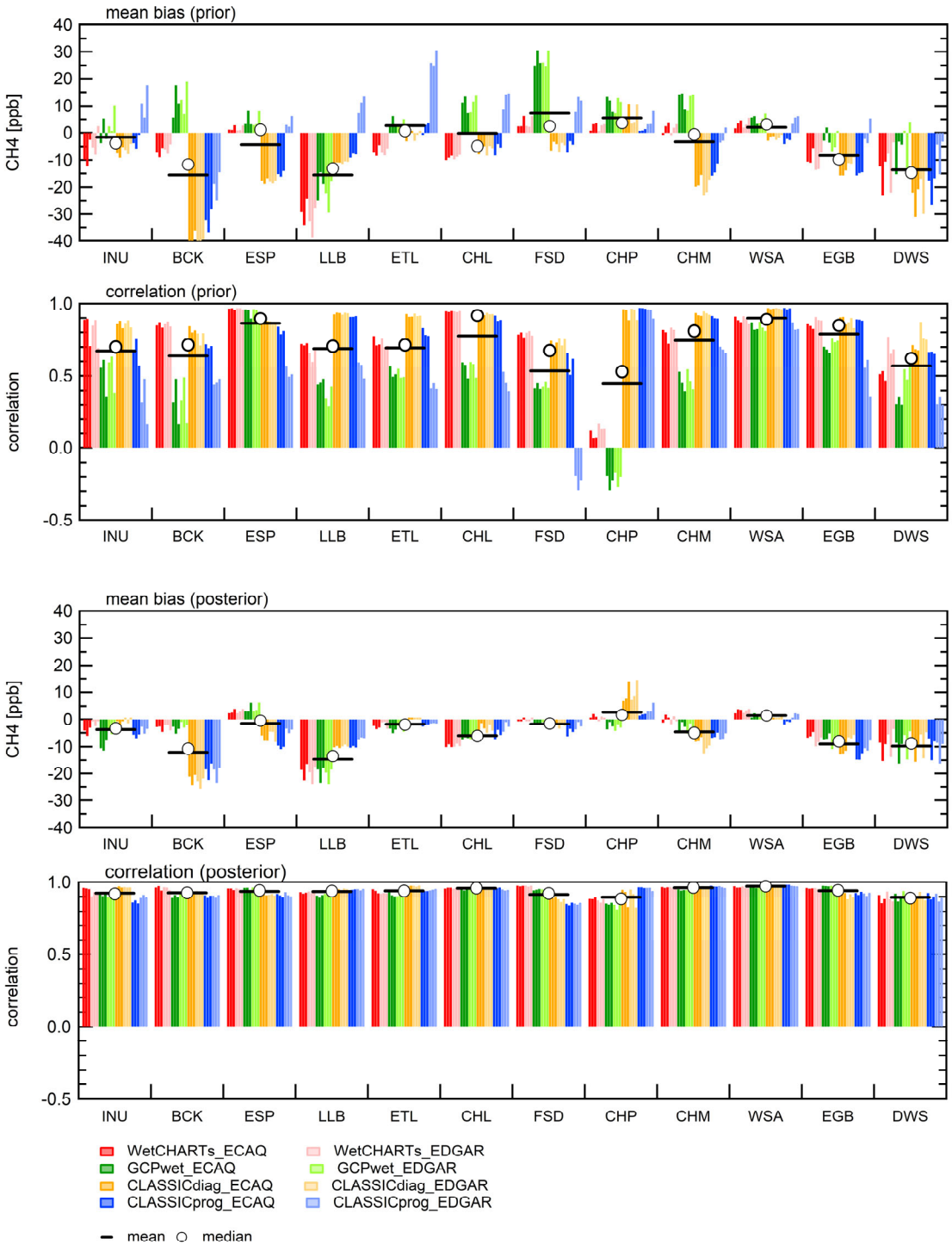


**Figure S7.** Annual mean bias and correlation between modelled (prior and posterior) mixing ratios and observations. The results of 24 experiments for the reference inversion (Inv_4R12S) are shown by site. The bar colours denote the respective prior emission scenarios. Three bars within each color denote the three different transport models; from left to right, FLEXPART_EI, FLEXPART_JRA and WRF-STILT.

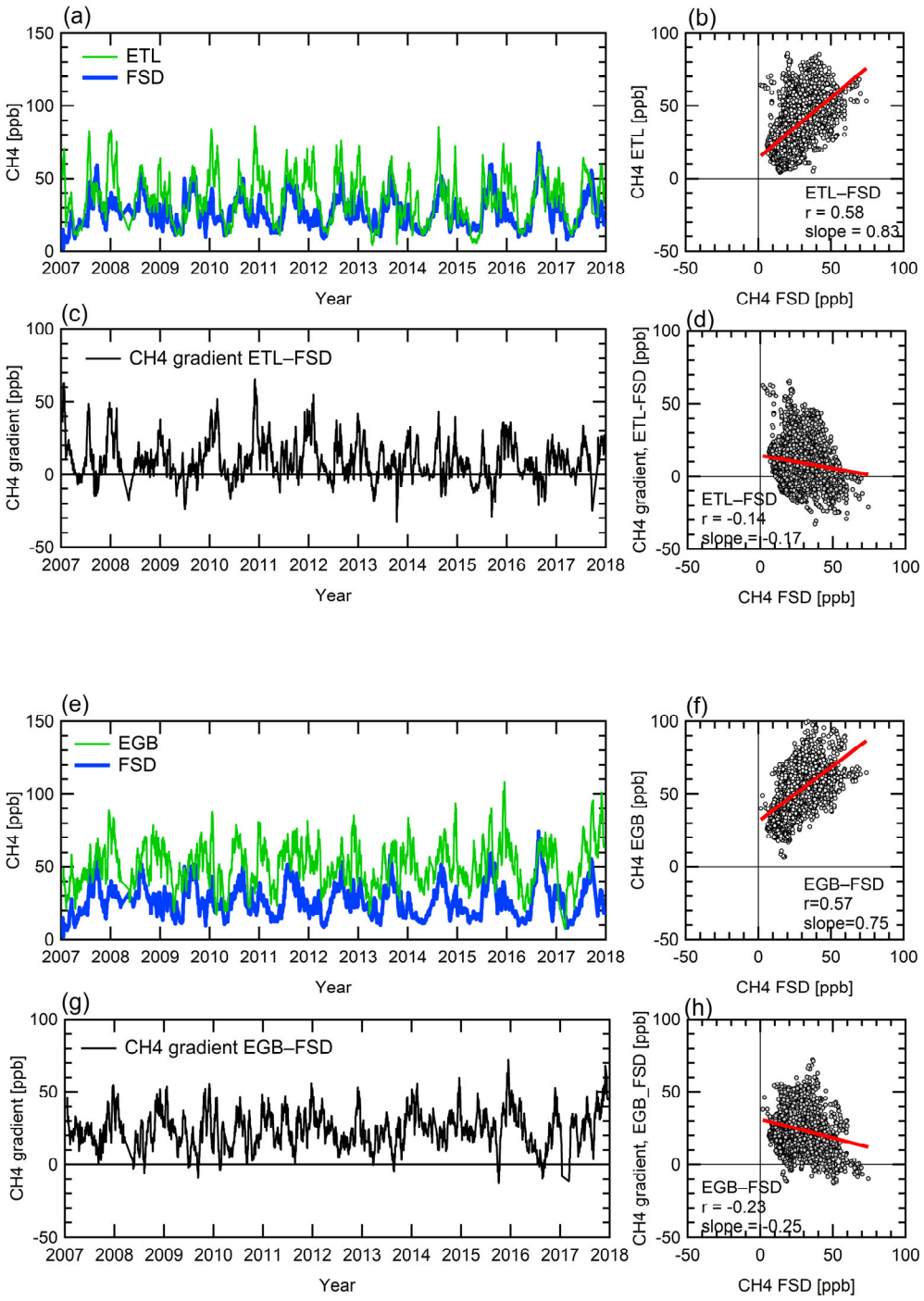


**Figure S8.** Examples of observational relationship between mixing ratio difference and the respective site mixing ratios. Upper: The case of ETL and FSD. FSD is used as a reference. (a) Time series of mixing ratios at ETL and FSD, from which the background mixing ratios are subtracted. (b) Correlation between mixing ratios at two sites. (c) Time series of the mixing ratio gradient between ETL and FSD (reference site), and (d) the correlation between mixing ratio gradient and mixing ratio at FSD. Lower: The case of EGB and FSD is shown in (e) to (h).

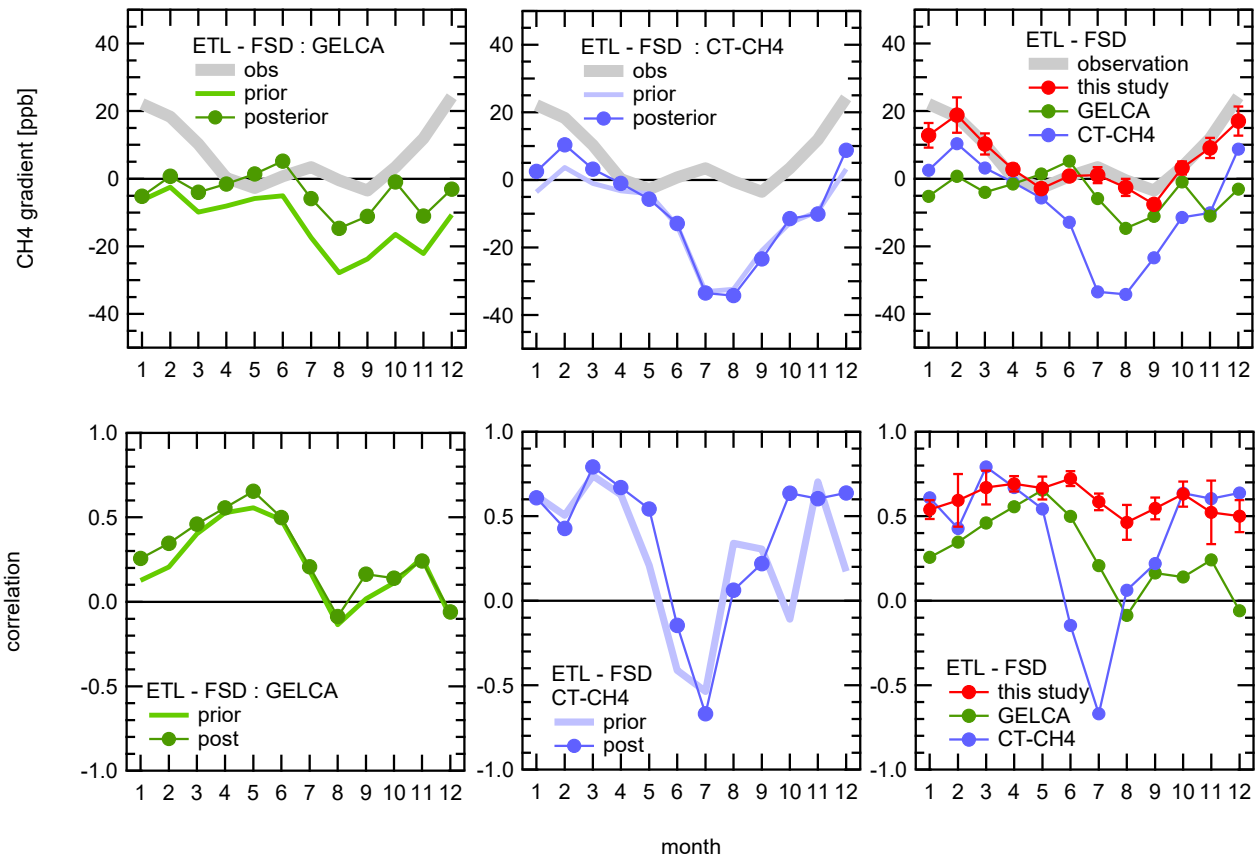


**Figure S9.** Gradients of modelled $CH_4$ mixing ratios between ETL and FSD (top) and the correlation (bottom): prior and posterior $CH_4$ mixing ratios modelled by global inverse models, GELCA (left) and CT-$CH_4$ (middle), compared with the observations. The right panels compare posterior $CH_4$ mixing ratio gradients among global models and this study.

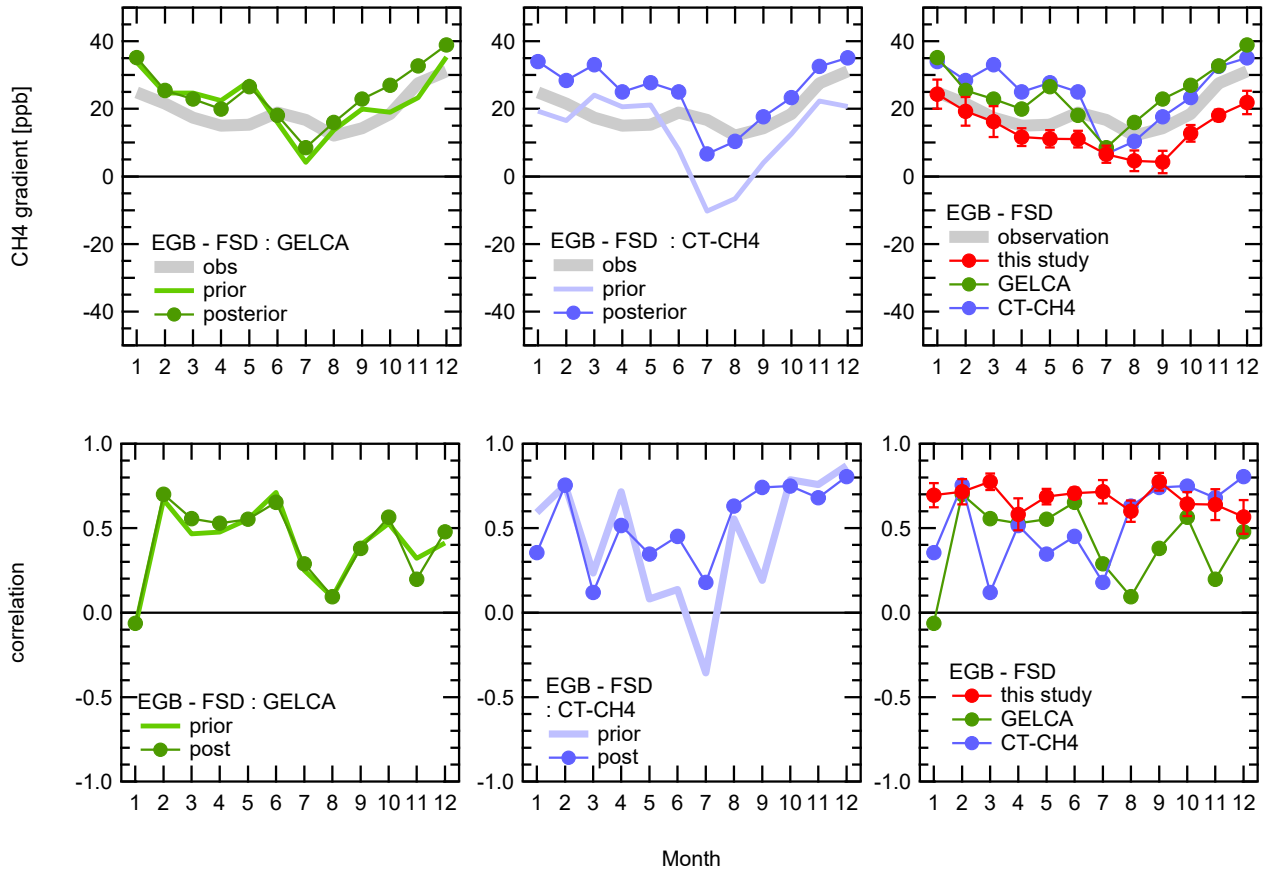


**Figure S9 (continued).** Same, but gradients of modelled $CH_4$ mixing ratios between EGB and FSD compared with the observations.

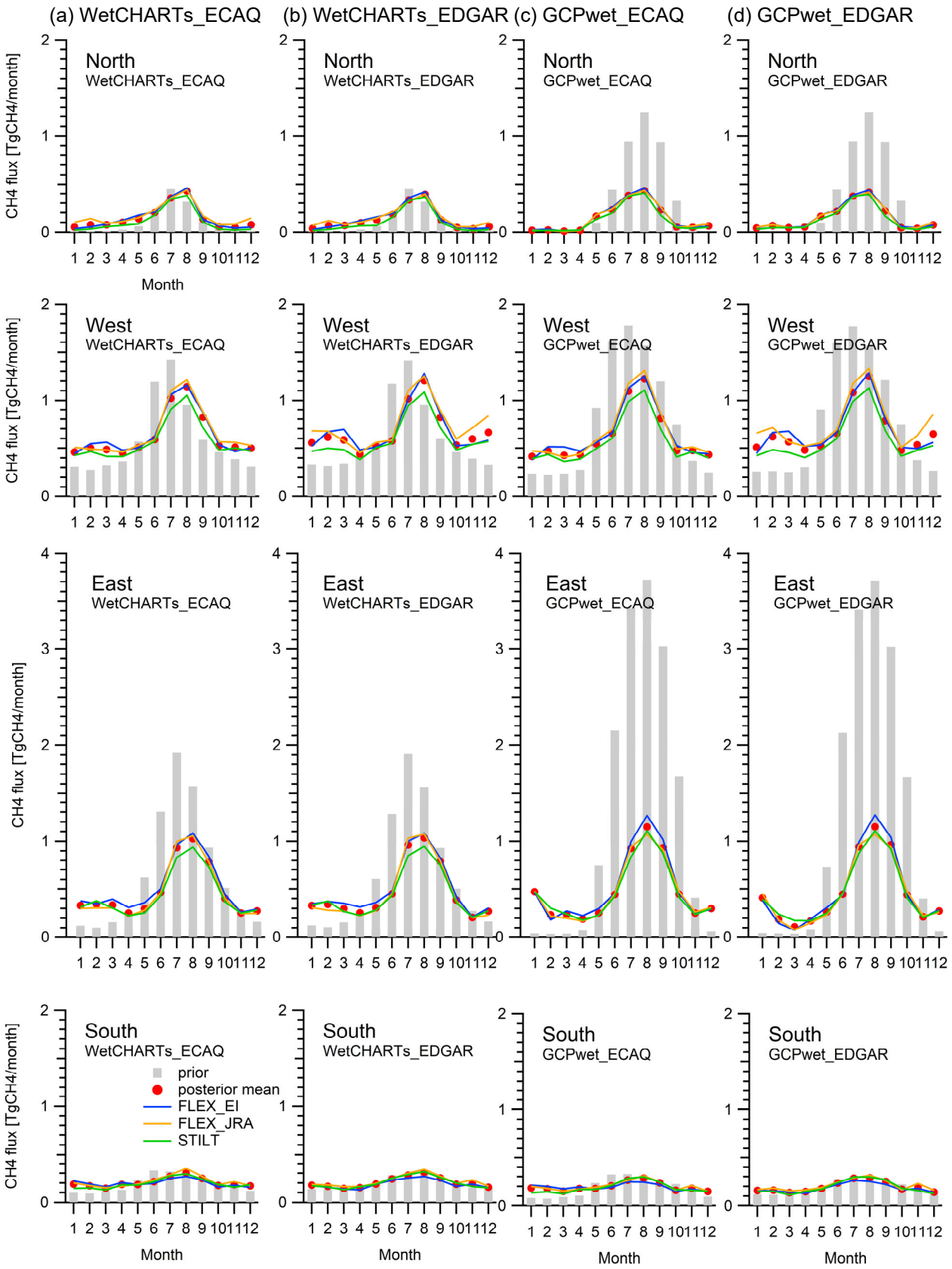


**Figure S10.** Mean subregional seasonal fluxes for 2012–2017 by 24 experiments in Inv_4R12S. Eight prior emission scenarios are shown with gray bars in (a), (b), (c), (d), (e), (f), (g) and (h), respectively. In each plot, blue, orange and green lines denote the mean flux estimates with the three different transport models, respectively, and the red line with circles is the mean over the estimates with the different transport models.

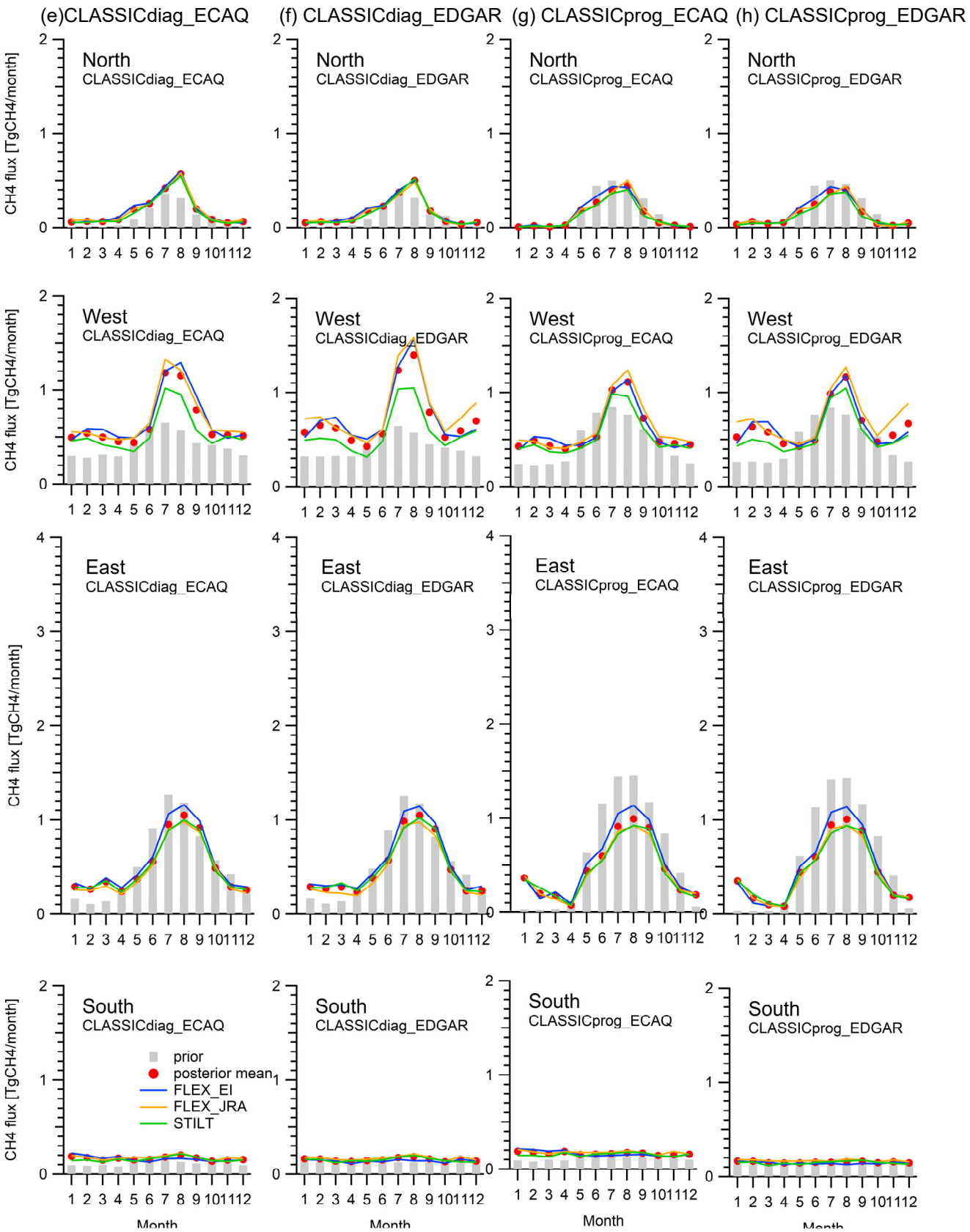


**Figure S10 (continued).** Mean seasonal fluxes for 2012–2017.

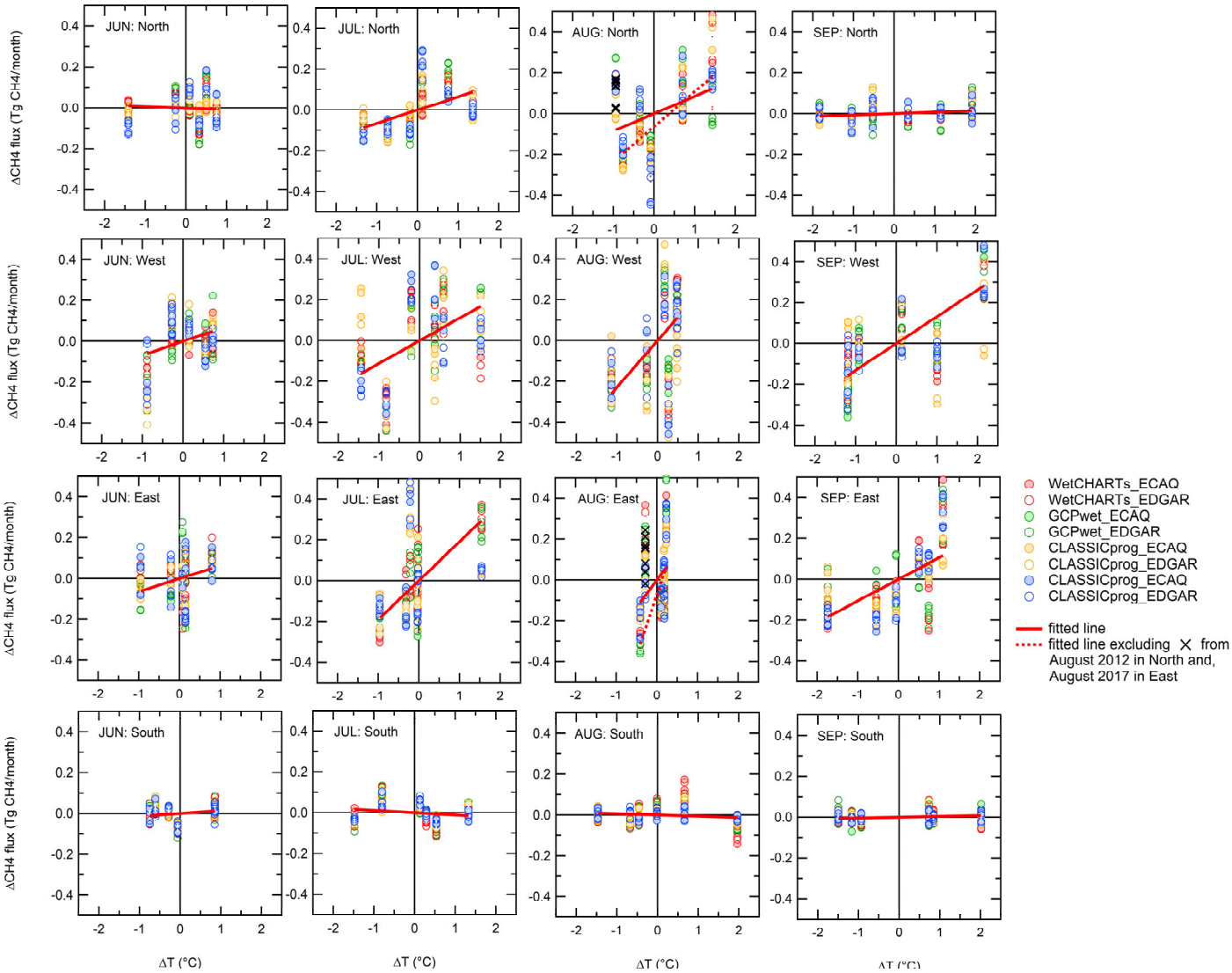


**Figure S11.** Flux-temperature relationship for summer months (June to September). Fluxes are monthly anomalies of posterior fluxes from the 6-year means (2012–2017) by subregion. Temperature anomalies are monthly deviations from the 6-year (2012–2017) means. The solid lines are the linear regressions with all the data points by month. The dotted lines are the linear regression when the data points for August 2014 in North, and August 2017 in East are excluded, respectively. The marker colours denote the different prior emission scenarios. The correlation coefficients of linear regressions are summarized in Table S4.

**Table S4**. Flux-temperature correlation coefficients in summer months by subregion. The values with brackets are obtained excluding the months when measurement sites inside a region experienced severe or lingering local forest fires: August 2014 in North and August 2017 in East.

| | June | July | August | September |
|---|---|---|---|---|
| North | 0.10 | 0.54 | 0.51 (0.81) | 0.41 |
| West | 0.38 | 0.50 | 0.47 | 0.75 |
| East | 0.28 | 0.54 | 0.40 (0.66) | 0.66 |
| South | 0.15 | -0.12 | -0.16 | 0.24 |

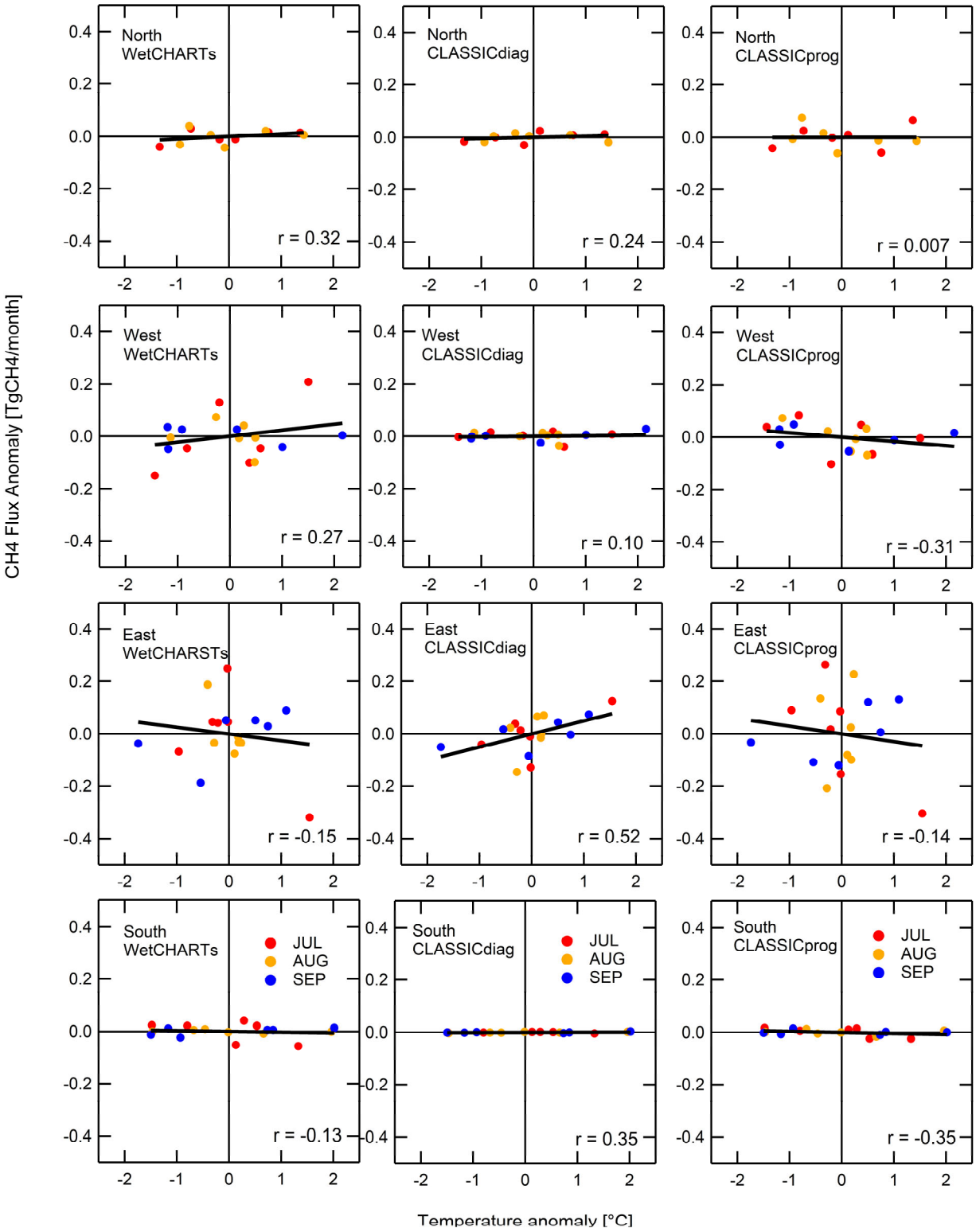


**Figure S12.** Prior wetland flux-temperature relationship in summer season for 2012–2017. Summer season is defined to be July to August for North, and July to September for the rest of subregions. The correlation analysis is applied to inter-annually varying prior wetland $CH_4$ fluxes, WetCHARTs (left column), CLASSICdiag (middle), and CLASSICprog (right).

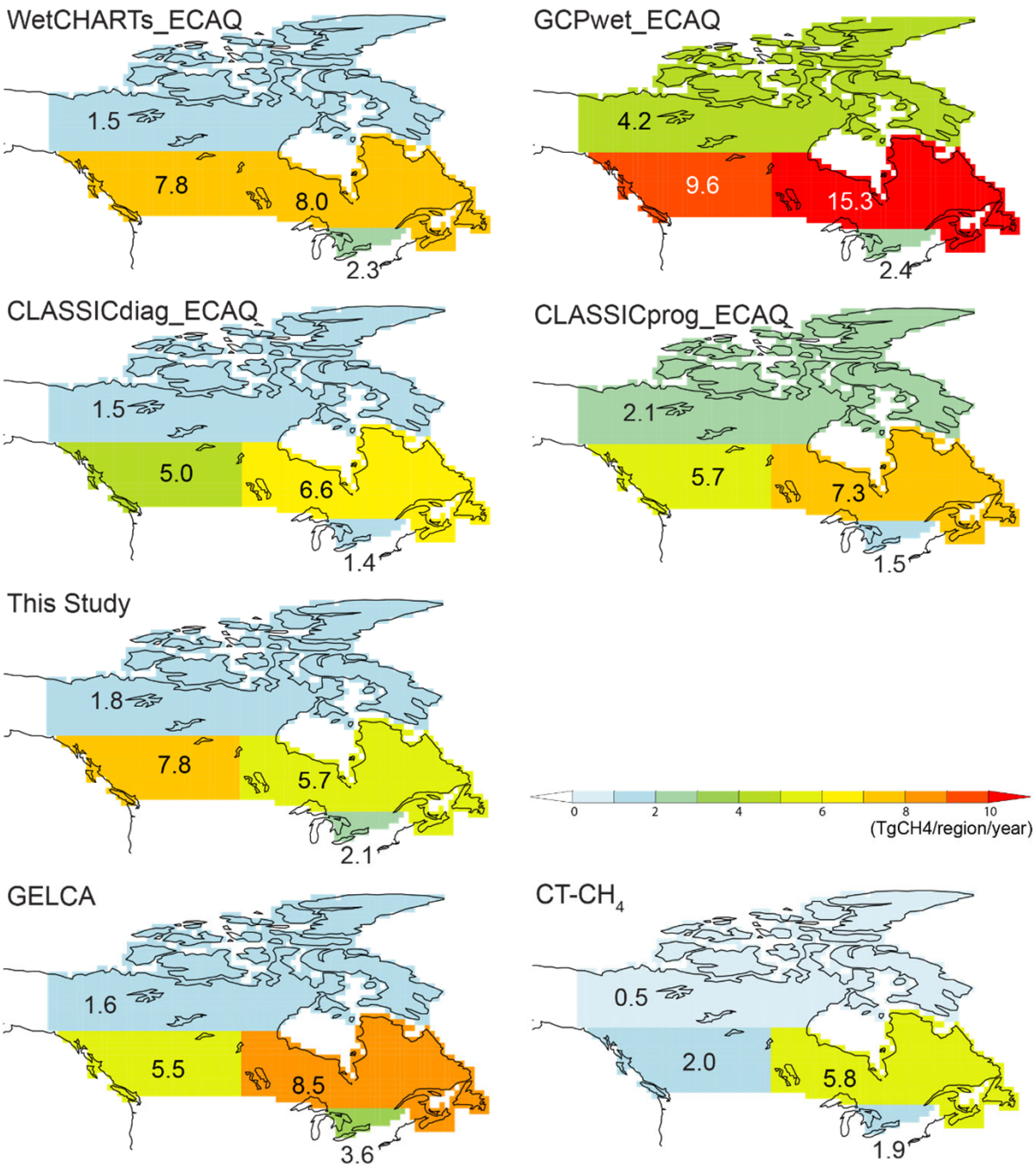


**Figure S13**. Spatial distribution of estimated mean total $CH_4$ emissions in the four subregions for 2012-2017. For the comparison, four out of the eight prior flux scenarios used in this study (WetCHARTs_ECAQ, GCPwet_ECAQ, CLSSSICdiag_ECAQ and CLASSICprog_ECAQ) are shown on the first and second tops, and estimates from global inversion studies, GELCA and CT-$CH_4$ on the bottom.

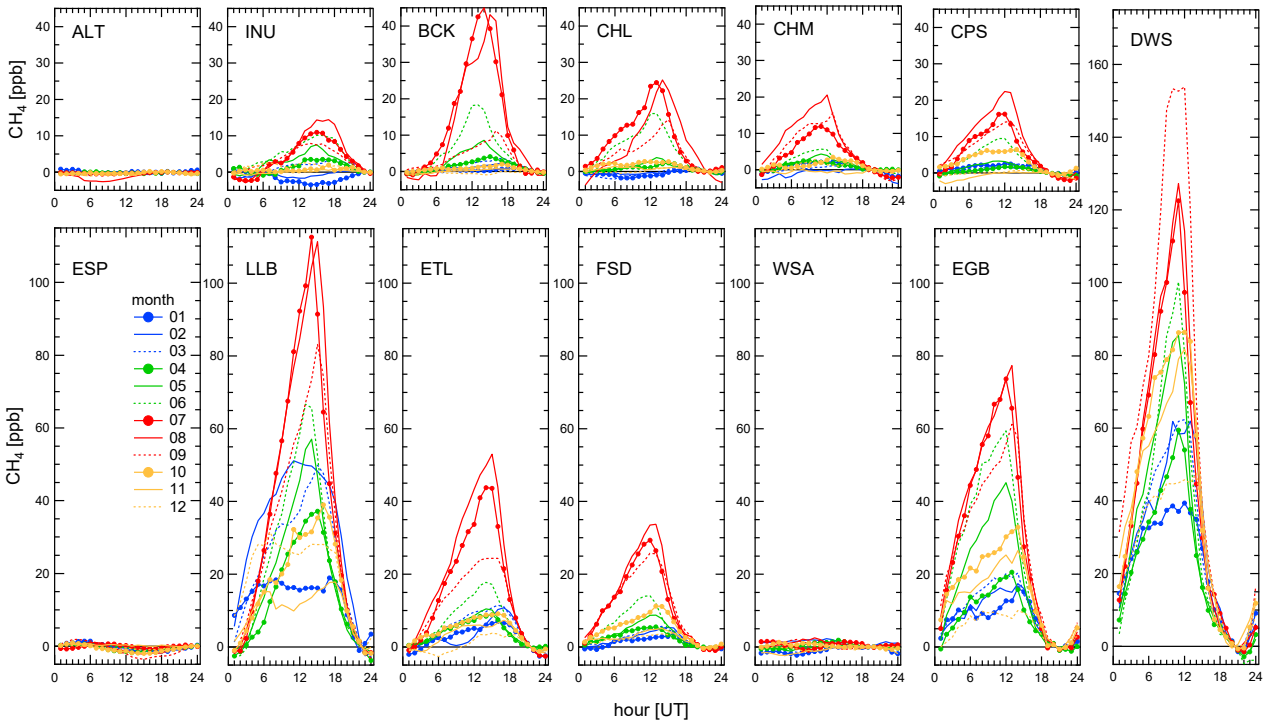


**Figure S14**. Monthly-averaged normalized diurnal cycles of observed atmospheric $CH_4$. Normalized diurnal cycles are derived with respect to the afternoon mean for 14:00–16:00 local time.